Nanoscale

Accepted Manuscript

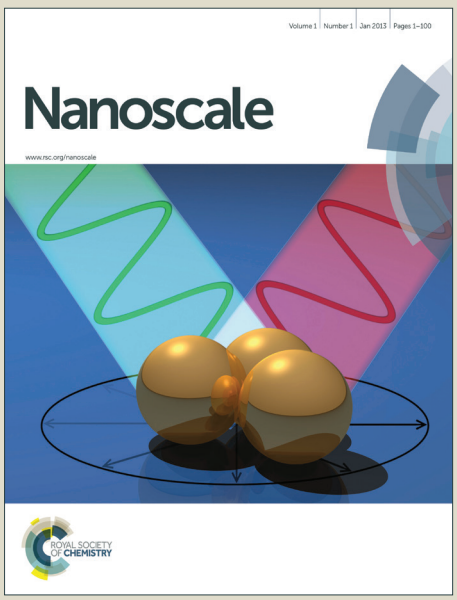

ROYAL SOCIETY OF CHEMISTRY

www.rsc.org/nanoscale

Effect of Substrate Discontinuities on the Propagating Surface Plasmon Polariton Modes in Gold Nanobars[†]

Paul Johns,[‡] Kuai Yu,[‡] Mary Sajini Devadas, Zhongming Li, Todd A. Major, and Gregory V. Hartland[§]

Department of Chemistry and Biochemistry

University of Notre Dame

Notre Dame, IN 46556-5670

[†] Electronic supplementary information (ESI) available: additional transient absorption images of SPP propagation in suspended gold nanobars and line profiles from the images. Field distributions for the different SPP modes as a function of gap size for rectangular nanobars with widths of 400 nm and 900 nm. The way the phase constants and propagation distances change with gap size for these nanobars are also presented.

[‡] These students contributed equally to this work.

[§] Corresponding author; e-mail: ghartlan@nd.edu

Abstract:

The surface plasmon polariton (SPP) modes of gold nanobars (nanowires with rectangular dimensions) have been investigated by scanning pump-probe microscopy. In these experiments the nanobars were suspended over trenches cut in glass coverslips, and propagating SPP modes were launched in the supported portion of the nanobar by focusing a near-IR pump laser beam at the end of the nanobar. Transient absorption images were then collected by scanning the probe laser over the nanobar using a galvo-mirror system. The images show that the trench has a large effect on the SPP modes, specifically, for approximately half the nanowires the propagation length is significantly reduced after the trench. Finite element calculations were performed to understand this effect. The calculations show that the pump laser excites bound and leaky modes (modes that have their fields localized at the nanobar/glass or nanobar/air interfaces, respectively) in the supported portions of the nanobars. These modes propagate along the nanobar. When they meet the trench their field distributions are altered. The modes that derive from the bound mode are strongly damped over the trench. Thus, the bound mode is not reconstituted on the opposite side of the trench, and only the leaky mode contributes to the signal. Because the bound and leaky modes can have different propagation lengths, the propagation lengths measured in our experiments can change from one side of the trench to the other. The results show how the substrate can be engineered to control the SPP modes in metal nanostructures.

Keywords: transient absorption microscopy, surface plasmon polaritons, mode conversion, finite element analysis, propagation length

Introduction:

Extended metal nanostructures, such as surfaces, wires or plates, can support Surface Plasmon Polariton modes (SPP modes), which are electromagnetic waves that propagate at the metal-dielectric interface.[1-5] The properties of the SPP modes depend on both the metal and the dielectric. For example, the mode symmetries, propagation lengths and wavevectors are different for metal nanowires in a homogeneous environment compared to nanowires supported on a substrate.[6, 7] Structure in the surface of the metal film or the supporting dielectric can also scatter the SPP modes, so that it is possible to engineer surface features to control their propagation.[8-18] SPPs also undergo mode conversion when encountering bends or branches.[19] In this process the electric and magnetic fields are redistributed around the nanowire. This effect has been used by various groups to create SPP power splitters,[20] aid transmission of SPPs over long distances,[21] and to demonstrate SPP logic operations and circuit functions.[22] Mode conversion also occurs when metal nanostructures are brought from a homogeneous environment onto a substrate, or vice versa. Understanding how SPPs interact with structured substrates is important for controlling SPP motion and developing plasmonic devices and sensors.[1-4, 23-25]

Most of our understanding of how SPPs interact with different dielectric substrates has come from theoretical studies.[9-18] Experiments have been limited, primarily because it is difficult to do repeated measurements on the same structure in different environments. Recently, we developed a technique to measure SPP propagation using pump-probe microscopy.[26, 27] In these experiments SPP modes are excited by focusing the pump laser at the end of the nanowire.[28-31] Scanning the probe laser over the structure while holding the pump fixed then yields an image of the SPP motion, which provides information about the propagation length and how the modes couple to different structures.[27] This technique provides a simple and repeatable way of interrogating SPP propagation in metal nanostructures and, as will be shown below, investigating substrate effects. Compared to other

techniques for studying SPP motion, it is easier to implement than near-field experiments,[32] provides more quantitative information than light scattering measurements,[28, 29] and allows multiple experiments on the same structure – which can be difficult in fluorescence detection measurements due to dye bleaching.[33-35]

In this study we use pump-probe microscopy to investigate propagation and mode conversion of SPPs in gold nanobars (nanowires with roughly rectangular cross-sections, lateral dimensions of hundreds of nanometers, and lengths of tens of microns) that were suspended over a trench in a glass surface. Only nanobars that span the trenches were interrogated. For these structures, two types of SPP modes are launched when the pump laser is focused on the end of the nanobar: a bound mode (designated as H_0) that propagates at the Au/glass interface, and a leaky mode (designated as H_2) that propagates at the Au/air interface.[7, 27, 36, 37] The transient absorption images provide information about the mode that has the longest propagation length. The relative propagation lengths of the bound and leaky modes depend on the dimensions of the nano-object.[37] Previously we found that in general the leaky mode H_2 has a longer propagation length and is detected in transient absorption measurements on larger nanobars (widths greater than 500 nm), whereas, the bound mode H_0 has a longer propagation length and is detected in smaller nanobars.[27] However, the exact value of the propagation length also depends on factors such as the aspect ratio of the nanobar (width divided by height), and the radius of curvature at the edges.[27] Here we show that discontinuities in the glass substrate have a strong effect on these SPP modes, causing changes in both the intensity and the form of the modes. The results from the experiments were compared to finite element calculations.[7, 27, 36-38] The calculations show that the bound mode is strongly damped over the trench, so that only the leaky mode is present on the far side of the trench. These results show how the substrate can be manipulated to create systems that support specific SPP modes.

Materials and Methods:

The gold nanobars used in this study were chemically synthesized using a modified literature protocol.[39] Briefly, 60 mL of n-pentanol with 1.5 g of solid polyvinylpyrrolidone (PVP, MW = 40,000 g/mol) was added to an Erlenmeyer flask, and stirred at room temperature for 30 min. 1.5 mL of a 0.024 M ethanol solution of $HAuCl_4 \cdot 3H_2O$ was slowly added down the side of the flask over 5 minutes. This was followed by the drop-wise addition of 1 mL of 0.01 M $HAuCl_4 \cdot 3H_2O$. After stirring for 5 min, the mixture was heated at 95°C in an oil bath, and kept at constant temperature for 24 hours. After the heating was discontinued, the solution was left undisturbed for four days. The obtained product was washed with ethanol three times by centrifugation and ultra-sonication. The washed samples were saved for later characterization and analysis. The gold nanobars produced have mostly rectangular cross-sections, with size distributions of 600 ± 220 nm, 380 ± 140 nm and 15 ± 4 μm for the width, height and length, respectively (errors equal standard deviation).[27] Representative Scanning Electron Microscopy (SEM) images of the sample are presented in the Supplemental Information, and SEM and Transmission Electron Microscopy images are presented in Ref. [[27]]. These images show that other shapes (such as nanobars with approximately pentagonal cross-sections) are also present in the sample.

The trenches were fabricated on the glass coverslips by photolithography and reactive ion-etching. The dimensions of the trenches were measured to be several hundred nm deep and several μm wide. Trenches with different widths were made during fabrication. The gold nanobars were spin-coated onto the glass substrate, and some of the gold nanobars were suspended over the trenches by chance. These nanobars were located by observing light scattering from the sample. Selected nanobars were examined by Atomic Force Microscopy (AFM) or SEM measurements. Representative AFM and SEM images of nanobars supported over trenches are shown in Figure 1. For the SEM experiment in Figure 1, the

sample was first coated by a thin layer of Ir to avoid charging – these coated samples were not used in the optical measurements. Correlated transient absorption/AFM measurements were performed by creating alignment markers on the glass substrate using microfabrication. Note that the AFM images give reliable information about the height and length of the structure, but are not accurate for analysis of the shape or width. Thus, only length and height information is given in the Figures presented below.

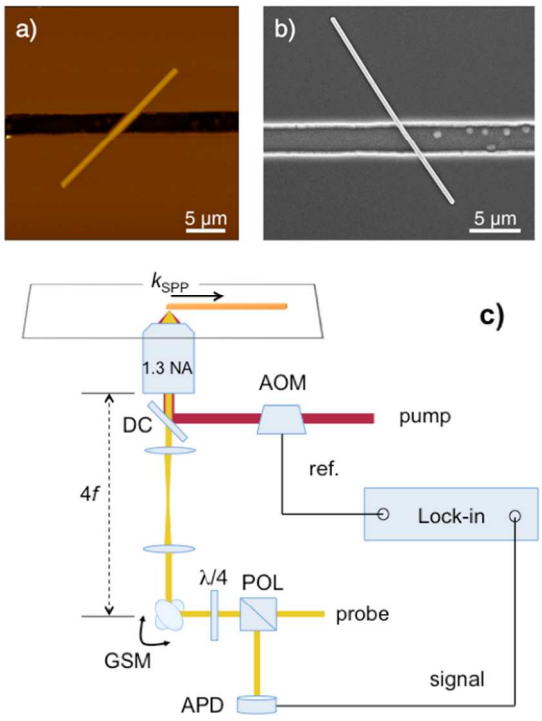

Figure 1. (a) Representative AFM image of a suspended gold nanobar over a trench on a glass substrate. (b) SEM image of a different nanobar. (c) Diagram of the experimental system. APD = avalanche photodiode; POL = polarizer; GSM = galvo-scanning mirror system; DC = dichroic mirror; AOM = acousto-optic modulator; λ/4 = quarter-wave plate; 4*f* = 4*f* lens system.

The scanning pump-probe microscopy experiments were performed using a Ti:sapphire oscillator/OPO laser system (80 MHz repetition rate). A diagram of the experimental setup is shown in Figure 1(c), and has been described in detail earlier.[26, 27] The pump beam was tuned to 800 nm and the probe beam from the OPO was 570 nm. The two beams were combined with a dichroic mirror, and then

focused at the sample with a high numerical aperture oil immersion objective (NA = 1.3). The experiments were performed in reflection, with an avalanche photodiode (APD) to detect the probe. A lock-in amplifier in conjunction with high frequency (400 kHz) modulation of the pump beam was used to extract the small change in reflectivity of the probe beam induced by the pump. The time delay between the pump and probe beams was controlled by a translation stage. In these experiments, the timing was set so that the pump and probe pulses are temporally overlapped. This maximizes the signal, and ensures that the measurement is not affected by processes such as heat diffusion along the nanobar. Half-wave plate/polarizer combinations were used to control the power of the pump and probe beams. The pump beam was linearly polarized and the polarization was aligned to be parallel to the long axis of the nanobar, while the probe beam was made circularly polarized with a quarter-wave plate. This allows us to pick-off the reflected probe with a polarizer – see Fig. 1(c). The pump and probe powers were kept below 800 μW and 200 μW, respectively. Under these conditions, the signal was stable and no melting or reshaping of the nanobars was observed, as confirmed by AFM measurements. Scattered light images of the nanobars were recorded with a CCD camera.

Propagating SPP modes were excited by focusing the pump beam at the end of a nanobar. To image SPP motion, the probe beam was spatially scanned relative to the pump beam using a two-dimensional galvo-scanning mirror (GSM) system.[26] A 4*f* lens system was constructed before the microscope using two 250 mm focal length lenses to direct the probe beam from the GSM to the back aperture of the objective. Typically, a 20 × 20 μm^2 image was recorded. The SPPs travel along the wire and as they move they dephase and create electron-hole excitations. The electron-hole excitations produce a transient absorption signal, and the number of electron-hole pairs depends on the SPP field strength.[27] Thus, the transient absorption signal gives a direct measurement of the SPP field at a given position on the nanobar. The propagation lengths of the SPP modes were determined by taking line

profiles along the nanobar, and fitting the transient absorption signal to an exponential decay. Sometimes we are not able to accurately fit the data to get a reasonable propagation length. In these cases the fit and propagation length were omitted.

COMSOL Multiphysics® (v4.4) was used to simulate infinitely long nanobars suspended in air or over a glass surface (index of refraction = 1.5), with gaps between the glass surface and the nanobar varying from 0–1500 nm. The simulations were performed on nanobars with square cross-sections with widths of 400 nm, 600 nm or 900 nm, and also on nanobars with a pentagonal cross-section. An interpolating function for the relative permittivity of gold was setup in COMSOL, using data from Johnson and Christy.[40] The glass and air layers were truncated using perfectly matched layers to eliminate reflections, and the corners of the nanobar were typically rounded with a radius of curvature of 10 nm. This rounding provides a more realistic geometry and avoids artifacts in the finite element analysis. The calculation domains were meshed with a custom triangular mesh and the mesh size was adjusted to ensure convergence of the propagation constant, which is defined as a wavevector $k_0 = \beta + i\alpha$, with β and α being the phase and attenuation constants, respectively. The wavevectors for each mode were determined using the Mode Analysis Study in COMSOL. The propagation length of a given mode can be found as $L = 1/(2\alpha)$.[7, 38]

Results and Discussion:

Figure 2 shows a transient absorption image of SPP propagation in a representative gold nanobar suspended over a trench. Figure 2(a) displays a scattered light image of the nanobar recorded with a lamp, and the corresponding AFM image that gives the nanobar dimensions is presented in the inset. The AFM image shows that the nanobar has a height of 340 ± 20 nm and a length of 20 μm, and that the trench has a width of 3 μm. A scattered light image of the SPP modes is presented in Figure 2(b). In

this experiment the SPPs were launched by focusing the 800 nm pump laser beam at the right end of the nanobar, and the scattered laser light was recorded with the CCD camera.[28, 29, 41] For the nanobar in Fig. 2, the leaky mode can be observed on both sides of the trench in the form of two lines located on either side of the nanobar.[36, 42] The trench clearly causes some light scattering (conversion of the SPP modes into photons), and attenuates the leakage radiation emitted by the nanobar. Figure 2(c) shows a transient absorption image of SPP propagation in the nanobar recorded for the pump laser parallel to the axis of the nanobar, and Fig. 2(d) shows a line profile of the signal along the nanobar. Note that the signal is on a natural log scale for both these panels, and also that the signal is smaller over the trench. This is because there is less reflection of the probe over the trench (see Fig. 2(a)).

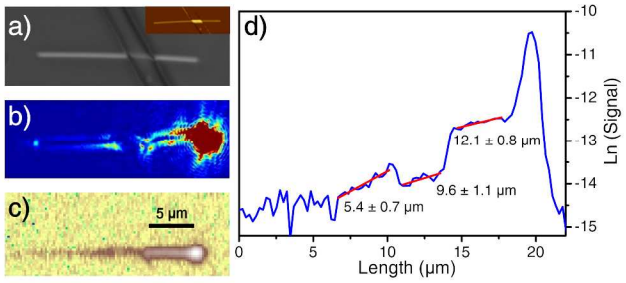

Figure 2. (a) White-light image of a gold nanobar suspended on a trench. Inset: AFM image of the gold nanobar. The nanobar has a length of 20 μm and a height of 340 ± 20 nm, and the trench is 3 μm wide. (b) False color scattered light image of the SPP modes for the nanobar. (c) Transient absorption image with pump excitation parallel to the long axis of the nanobar. (d) Line profile of the signal extracted from the image in panel (c). Note that the intensities are on a log scale. Fits to the data (red lines) give estimates of the SPP propagation lengths (which are given in the Figure).

The transient absorption data in Figs. 2(c) and (d) shows that the trench has a large effect on the intensity of the signal created by the SPP modes, as well as their propagation length. The propagation lengths in the different regions of the nanobar were determined by fitting the line profile to an exponential decay. For the supported portions of the nanobar the propagation length changes from 12.1 ± 0.8 μm on the side near the pump beam, to 5.4 ± 0.7 μm on the opposite side of the trench. Note that the change in the propagation length does not depend on whether the nanobar is excited on the left or

right. This is demonstrated in Figure 3, which shows transient absorption images and line profiles for an experiment where the pump laser was positioned at either end of a different nanobar. The change in propagation length for the supported portions on either side of the trench is unexpected, and shows that there is a change in the SPP mode being detected. The propagation length is also different over the trench, but this is less surprising as nanobars in a homogeneous environment support different SPP modes – which have different propagation lengths – than nanobars on a substrate.[7, 27, 43, 44]

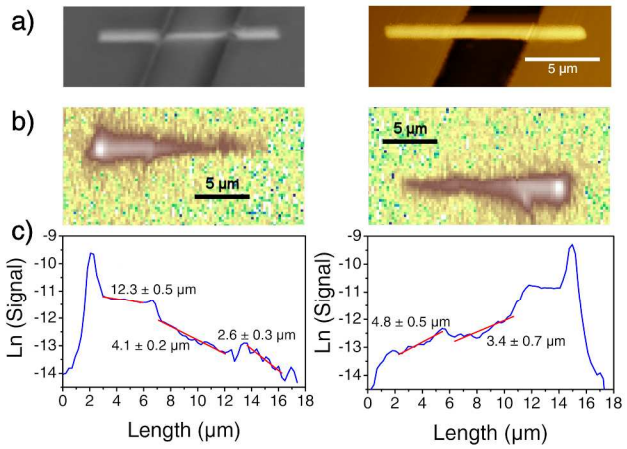

Figure 3: (a) Scattered light and AFM images of a gold nanobar suspended over a trench. The nanobar has a length of 13 μm and a height of 590 ± 20 nm, and the trench is 4.8 μm wide. (b) Transient absorption microscopy images of the gold nanobar with pump laser excitation at either end of the structure. The pump polarization was parallel to the long axis of the nanobar. (c) Line profiles of the signal extracted from the images in part (b). The data shows that for this nanobar the SPP propagation length is significantly shorter on the far side of the trench, irrespective of which end is excited.

Note that not all the nanobars investigated show differences in the propagation length for the two sides of the trench. Figure 4 shows an example where the propagation length is similar on both sides of the trench. For the nanobar in Figure 4 there is also a smaller loss in signal across the trench.

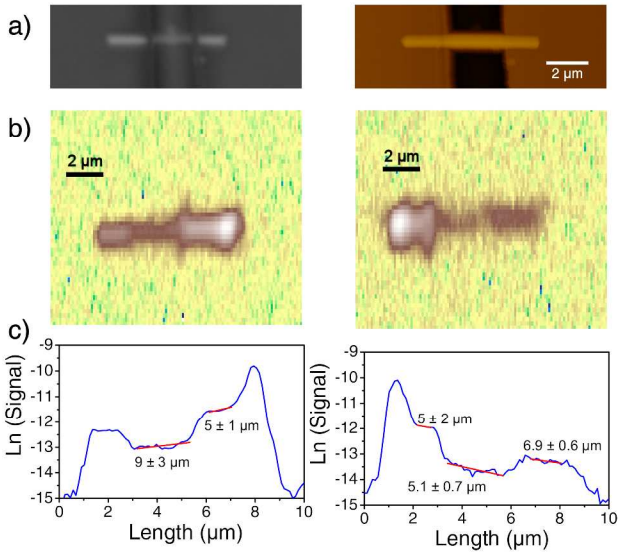

Figure 4. (a) White-light image of a gold nanobar suspended over a trench. Inset: AFM image that gives a length of 6.6 μm for the nanobar and a height of 310 ± 10 nm. The trench is 2.5 μm wide. (b) Transient absorption images with pump excitation parallel to the long axis of the nanobar. (c) Line profiles of the signal extracted from the images in part (b).

The observation that the propagation length for the supported portion of the nanobar can be different on the near and far sides of the trench is the major result of this work. Qualitatively, this result can be understood in the following way: the pump laser excites both the bound and leaky modes, and the transient absorption signal reports on the mode with the longest propagation length – which can be either the bound or the leaky mode.[27] The SPP scattering image in Figure 2(b) shows that the leaky mode can propagate across the trench. Assuming that the bound mode is strongly attenuated by the trench, cases where there is a change in propagation length on the two sides of the trench can be explained by the bound mode dominating the signal on the near side of the trench, and the leaky mode dominating on the far side. In contrast, cases where the propagation length is the same on both sides of the trench could arise when the leaky mode dominates the signal on both sides of the trench, or the bound and leaky modes have similar propagation lengths (which can happen for certain dimensions, see Ref. [[27]]).

To provide a more quantitative understanding of SPP propagation in these systems, Finite Element calculations were performed for nanobars suspended above a glass surface with gap sizes ranging from 0–1500 nm between the bar and the surface. By gradually varying the size of the gap, the way the SPP modes are transformed when they reach the trench can be studied. For these calculations a mode analysis was done in COMSOL and, from this, the complex wavevector of each mode was determined, giving values for the propagation constant β and the propagation length. Figure 5 shows field plots and values for β and the propagation length L_{SPP} for the various modes supported by a nanobar with a square cross-section and a width of 600 nm, which corresponds to the average width of the nanobars interrogated in our experiments. Data for square nanobars with widths of 400 nm and 900 nm can be found in the Supplemental Information.

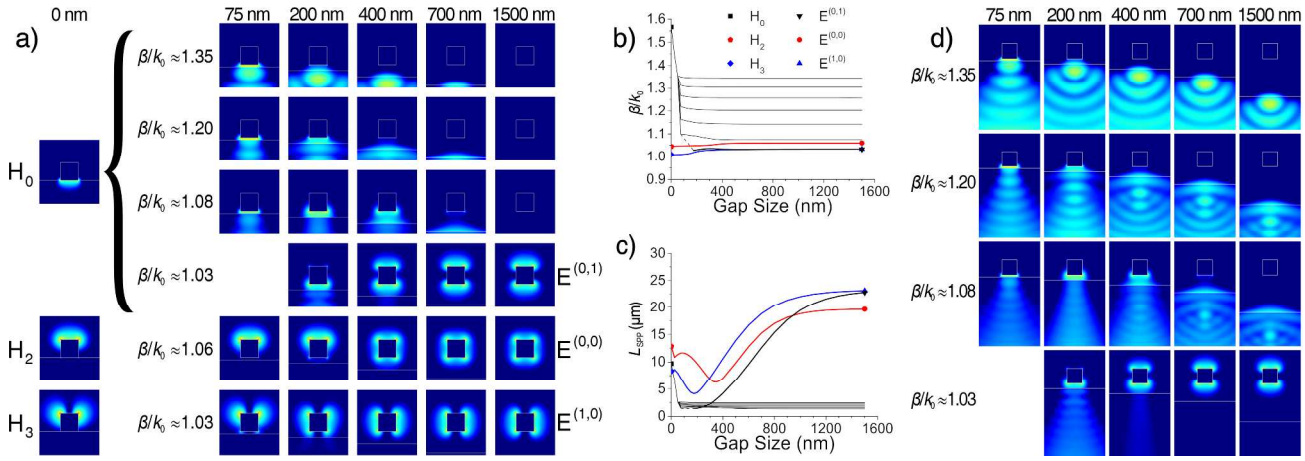

Figure 5.Field plots for a selection of the different modes for a square nanobar with an edge length of 600 nm at different gap sizes (intensities are on a log scale). The white horizontal line indicates the air/glass interface. Beginning at 75 nm gap size, the H_0 mode breaks into several branches, each involving both the nanobar and the glass to varying degrees. For the modes derived from the H_0 mode, the branch with the lowest β value transforms into the $E^{(0,1)}$ mode (black line in panels (b) and (c)). The H_2 mode transforms into the $E^{(0,0)}$ mode with increasing gap size (red line), while the H_3 mode transitions to the $E^{(1,0)}$ mode (blue line). (b) Phase constants and (c) propagation lengths for the SPP modes. (d) Field plots for four selected branches of the H_0 mode presented over a larger size range to show the contribution from the glass.

The field patterns for the different modes are shown in Figure 5(a) for a selection of different gap sizes. The modes are labeled by their β/k_0 values at a gap size of 400 nm, the smallest distance at which β remains relatively constant (see Figure 5(b)). When the nanobar is in contact with the substrate (0 nm gap size), the modes can be identified and labeled using the nomenclature for substrate supported nanowires: that is, as H_0, H_1, H_2, and H_3.[7, 37] Note that the H_1 mode has a cutoff value and is not found for nanobars with widths of 400 nm or 600 nm (images of the H_1 mode for a 900 nm wide square nanobar are presented in the Supplemental Information). Similarly, at large gap sizes the modes can be identified and labeled using the nomenclature for square SPP waveguides in a homogeneous environment: $E^{(0,0)}$, $E^{(1,0)}$, $E^{(0,1)}$ and $E^{(1,1)}$.[43, 44] Plotting the values of β as a function of gap size, and examining the field plots, allows us to determine how the SPP modes for the supported nanobars transform when they meet the trench. First, the H_3 mode transitions into the $E^{(1,0)}$ mode with increasing gap size. This can be seen by following both the β/k_0 and L_{SPP} values as a function gap size, and from inspecting the field plots. This mode is excited when the probe laser is perpendicular to the long axis of the nanobar, and is not relevant to our experiments. Likewise, the leaky mode (H_2) transforms into the $E^{(0,0)}$ mode. As the gap between the nanobar and the glass increases, the field for the leaky mode becomes less localized at the top of the nanobar, and begins to spread out, eventually becoming symmetric around the nanobar. At large gap sizes the field distribution is analogous to that for the $E^{(0,0)}$ mode. In contrast, the bound mode transforms into a series of modes with different β/k_0 values.

Figure 5(d) shows mode plots, beginning at a gap size of 75 nm, for several of the modes that are connected to the bound mode (the modes are again labeled by their β/k_0 values). These plots are over a larger area than those in Figure 5(a), to emphasize the role of the substrate. The different branches involve different contributions from the glass substrate and the gold nanobar. The branch with the lowest β value ($\beta/k_0 \approx 1.03$) evolves into the $E^{(0,1)}$ mode as the gap size increases. Note we were not able to

identify the $\beta/k_0 \approx 1.03$ mode for gap distances smaller than approximately 200 nm. Figure 5 shows that at gap sizes greater than 400 nm, only the $\beta/k_0 \approx 1.03$ mode has a significant contribution from the nanobar. Thus, this mode would be the one that primarily contributes to the transient absorption signal over the trench. For all the other modes that derive from the H_0 mode, the fields become localized in the glass. The size of the gap required for the fields to become localized in the glass depends on the width of the nanobar. For smaller nanobars this localization occurs at a smaller gap size, and for larger nanobars it occurs at a larger gap size (see Supplemental Information). Note that there are many more glass modes than those shown in Figure 5. The modes presented here are the ones that we can connect to the bound mode. Also note that the $\beta/k_0 \approx 1.03$ mode that derives from the bound mode is leakier than the leaky mode, that is it has a smaller propagation constant than the H_2 mode,[37] for gap sizes larger than 200 nm.

At large gap sizes (greater than 1500 nm), the modes that involve fields in the nanobar have phase constants and propagation lengths identical to those for the $E^{(0,0)}$, $E^{(0,1)}$ and $E^{(1,0)}$ modes for a nanobar in air, see Figure 5.[43, 44] At this gap size the glass substrate has no effect on the SPP modes of the nanobar. For the gap sizes relevant to our experiments (several hundred nm), all of the modes that are derived from the bound mode have short propagation lengths (less than 3 μm) and, thus, will be strongly damped over the trench. This implies that the bound mode will not survive the interaction with the trench. On the other hand, the propagation length for the mode that derives from the leaky mode (H_2) is on the order of 5 – 10 μm for gap sizes of a few hundred nanometers. Thus, this mode will survive the 2.5 – 5 μm wide trenches, albeit with some damping.

The theoretical analysis presented above provides the following picture for the fate of the bound and leaky modes as they interact with the trench: The leaky mode transforms into a mode that has a similar form as the $E^{(0,0)}$ mode for a nanobar in a homogeneous environment. When this mode reaches

the opposite side of the trench, it converts back to the leaky mode, but with some attenuation due to Joule losses that depend on the exact dimensions of the nanobar and the trench depth. In contrast, the bound mode is transformed into a series of modes that involve both the glass and the nanobar. These modes are strongly damped and do not survive across the trench, which means that the bound mode is not reconstituted on the opposite side of the trench. Thus, in our transient absorption experiments the leaky mode is always measured on the far side of the trench, but either the leaky or the bound mode can dominate the response on the near side – depending on which has a longer propagation length.[27]

Our previous simulations for rectangular nanobars on a glass surface showed that the bound mode has a longer propagation length than the leaky mode, and therefore is expected to dominate the transient absorption response, for nanobars with heights less than approximately 500 nm,[27] whereas, the leaky mode dominates (has a longer propagation length) for larger nanobars. (The exact values also depend on the aspect ratio and the radius of curvature of the structure.[27]) Using the analysis given above, the results in Figure 2 can be explained as follows: this nanobar is a relatively small structure where the bound mode has a longer propagation length than the leaky mode over the glass (see Figure S4). The bound mode dominates the signal on the near side of the trench (because it has a longer propagation length), but it is strongly damped by the trench, causing a change in the measured propagation length from long to short across the trench. Likewise, the data in Figure 4 can be explained as arising from a structure where the dimensions (height, aspect ratio and radius of curvature at the edges) are such that the leaky mode has either a similar or longer propagation length than the bound mode for the structure on glass.[27] In this case there would be no change in the measured propagation length from one side of the trench to the other.

However, using this logic, it is difficult to explain cases such as those in Figure 3 and Figure S1 in the Supplemental Information, where a change in propagation length is measured for nanobars with

larger sizes. This implies that another effect is playing a role in these measurements, and we believe that this is shape. SEM images of the samples used in these experiments show that there are a variety of different shapes present, see the Supplemental Information and also Ref. [27]. To investigate the effect of shape, simulations for a pentagonal nanobar were performed and are presented in Figure 6. This is a common shape seen in chemically synthesized nanowires.[45-48] The dimensions in the FE simulations were chosen to match those of the nanostructure in Figure 3. For the supported structure in Figure 6 (0 nm gap), the bound mode localized at the metal/glass interface has a longer propagation length than the mode at the metal/air interface. Like what happens for the square nanobars, the bound mode breaks up into a series of modes over the trench, that are strongly damped. These modes will be extinguished by the trench. The mode at the metal/air interface transforms into a more symmetric mode over the trench, that has a propagation length that is long enough to survive the trench. Thus, in this system the measured propagation length in the transient absorption measurements would change from long to short across the trench, consistent with the results of Figure 3.

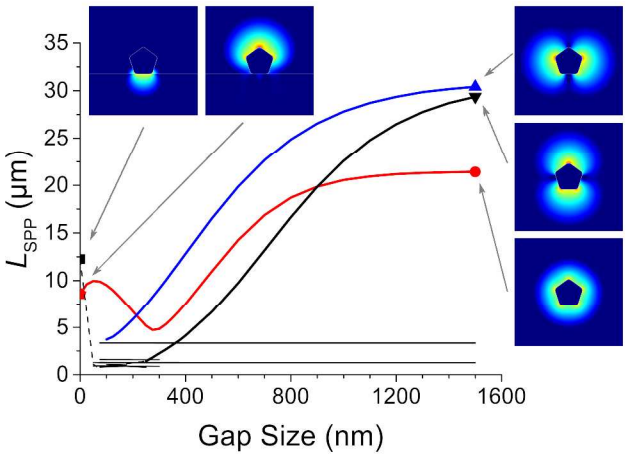

Figure 6. Propagation lengths L_{SPP} for the SPP modes of a pentagonal nanobar with a height of 590 nm and a 75 nm radius of curvature at the edges. This height is consistent with the AFM measurements for the nanobar in Figure 3. For the modes of the suspended nanobar that derive from the bound mode, the mode with the largest contribution from the nanobar is shown as a thick black line, while the other branches are shown as thinner black lines. Field plots for the modes for the nanobar on the glass surface, and for a large gap size are also shown. These modes are consistent with those discussed in Ref. [36].

Summary and Conclusions

We have used scanning pump-probe microscopy and finite element analysis to examine how SPP modes in chemically synthesized gold nanobars propagate across trenches in a substrate. In these experiments both the bound and leaky modes are launched in the supported portion of the nanobar. When these modes reach the edge of the trench they transform into modes that involve the nanobar (for the leaky mode) and the nanobar and the surface (for the bound mode). The modes in the trench region that are derived from the bound mode are strongly damped, and do not reach the other side of the trench. Thus, the trench effectively eliminates the bound mode, so that on the far side of the trench only the leaky mode is present. This work shows how the substrate can be engineered to control the form of the SPP modes in metal nanostructures, which is relevant both to creating plasmonic devices that perform different functions and for amplifying SPP modes in metal nanostructures.

Acknowledgments: This work was supported by the National Science Foundation (CHE-1110560), the Office of Naval Research (Award No.: N00014-12-1-1030), and the University of Notre Dame Strategic Research Initiative. Computational time was provided by the Center for Research Computing (CRC) at the University of Notre Dame.

TOC Graphic:

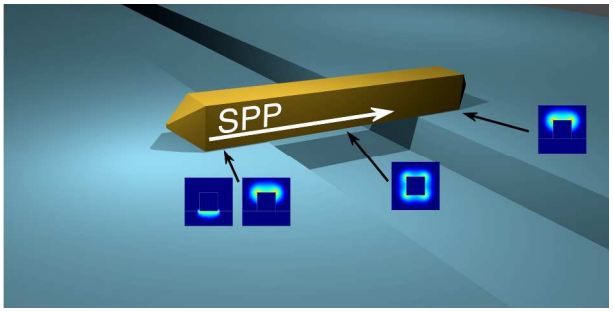

References:

1. S. I. Bozhevolnyi, *Plasmonic Nanoguides and Circuits*, Pan Stanford Publishing Pte. Ltd., 2008.
2. W. L. Barnes, A. Dereux and T. W. Ebbesen, *Nature*, 2003, 424, 824-830.
3. W. A. Murray and W. L. Barnes, *Advanced Materials*, 2007, 19, 3771-3782.
4. T. W. Ebbesen, C. Genet and S. I. Bozhevolnyi, *Phys. Today*, 2008, 61, 44-50.
5. T. A. Major, M. S. Devadas, S. S. Lo and G. V. Hartland, *Journal of Physical Chemistry C*, 2013, 117, 1447-1452.
6. P. Berini, *Phys. Rev. B*, 2000, 61, 10484-10503.
7. S. Zhang and H. Xu, *ACS Nano*, 2012, 6, 8128-8135.
8. S. I. Bozhevolnyi and V. Coello, *Physical Review B*, 1998, 58, 10899-10910.
9. J. A. Sánchez-Gil, *Appl. Phys. Lett.*, 1998, 73, 3509-3511.
10. F. López-Tejeira, F. J. García-Vidal and L. Martín-Moreno, *Applied Physics A*, 2007, 89, 251-258.
11. A. Y. Nikitin, F. Lopez-Tejeira and L. Martin-Moreno, *Physical Review B*, 2007, 75, 035129.
12. R. F. Oulton, D. F. P. Pile, Y. Liu and X. Zhang, *Physical Review B*, 2007, 76, 035408.
13. M. Kuttge, F. J. G. de Abajo and A. Polman, *Opt. Express*, 2009, 17, 10385-10392.
14. B. Baumeier, F. Huerkamp, T. A. Leskova and A. A. Maradudin, *Phys Rev A*, 2011, 84, 013810.
15. G. Brucoli and L. Martin-Moreno, *Physical Review B*, 2011, 83, 075433.
16. G. Y. Li, F. Xiao, L. Cai, K. Alameh and A. S. Xu, *New Journal of Physics*, 2011, 13, 073045.
17. R. E. Arias and A. A. Maradudin, *Opt. Express*, 2013, 21, 9734-9756.
18. J. Polanco, R. M. Fitzgerald and A. A. Maradudin, *Physical Review B*, 2013, 87, 155417.
19. D. Pan, H. Wei, Z. Jia and H. Xu, *Scientific Reports*, 2014, 4, 4993.
20. M. S. Kumar, X. Piao, S. Koo, S. Yu and N. Park, *Opt. Express*, 2010, 18, 8800-8805.
21. S. Sun, H. T. Chen, W. J. Zheng and G. Y. Guo, *Opt. Express*, 2013, 21, 14591-14605.
22. W. H. Dai, F. C. Lin, C. B. Huang and J. S. Huang, *Nano Letters*, 2014, 14, 3881-3886.
23. M. Cohen, Z. Zalevsky and R. Shavit, *Nanoscale*, 2013, 5, 5442-5449.
24. M. T. Sun, Y. X. Hou and H. X. Xu, *Nanoscale*, 2011, 3, 4114-4116.
25. S. Lal, J. H. Hafner, N. J. Halas, S. Link and P. Nordlander, *Acc. Chem. Res.*, 2012, 45, 1887-1895.
26. S. S. Lo, H. Y. Shi, L. Huang and G. V. Hartland, *Optics Letters*, 2013, 38, 1265-1267.
27. K. Yu, M. S. Devadas, T. A. Major, S. S. Lo and G. V. Hartland, *J. Phys. Chem. C*, 2014, 118, 8603-8609.
28. R. M. Dickson and L. A. Lyon, *J. Phys. Chem. B*, 2000, 104, 6095-6098.
29. A. W. Sanders, D. A. Routenberg, B. J. Wiley, Y. N. Xia, E. R. Dufresne and M. A. Reed, *Nano Letters*, 2006, 6, 1822-1826.
30. H. Staleva and G. V. Hartland, *Journal of Physical Chemistry C*, 2008, 112, 7535-7539.
31. H. Staleva, S. E. Skrabalak, C. R. Carey, T. Kosel, Y. Xia and G. V. Hartland, *Phys. Chem. Chem. Phys.*, 2009, 11, 5889-5896.
32. B. Lamprecht, J. R. Krenn, G. Schider, H. Ditlbacher, M. Salerno, N. Felidj, A. Leitner, F. R. Aussenegg and J. C. Weeber, *Appl. Phys. Lett.*, 2001, 79, 51-53.
33. D. Solis, W.-S. Chang, B. P. Khanal, K. Bao, P. Nordlander, E. R. Zubarev and S. Link, *Nano Lett.*, 2010, 10, 3482-3485.
34. D. Solis, Jr., A. Paul, W.-S. Chang and S. Link, *Journal of Physical Chemistry B*, 2013, 117, 4611-4617.
35. B. Wild, L. N. Cao, Y. G. Sun, B. P. Khanal, E. R. Zubarev, S. K. Gray, N. F. Scherer and M. Pelton, *ACS Nano*, 2012, 6, 472-482.
36. M. Song, A. Bouhelier, P. Bramant, J. Sharma, E. Dujardin, D. Zhang and G. Colas-des-Francs, *ACS Nano*, 2011, 5, 5874-5880.
37. R. Zia, M. D. Selker and M. L. Brongersma, *Phys. Rev. B*, 2005, 71, 165431.
38. H. Wei, S. P. Zhang, X. R. Tian and H. X. Xu, *Proc. Natl. Acad. Sci. U. S. A.*, 2013, 110, 4494-4499.
39. J. H. Zhang, H. Y. Liu, Z. L. Wang and N. B. Ming, *Applied Physics Letters*, 2007, 91, 133112.
40. P. B. Johnson and R. W. Christy, *Physical Review B*, 1972, 6, 4370-4379.
41. G. I. Stegeman, R. F. Wallis and A. A. Maradudin, *Optics Letters*, 1983, 8, 386-388.

42. T. Shegai, V. D. Miljkovic, K. Bao, H. Xu, P. Nordlander, P. Johansson and M. Kall, *Nano Letters*, 2011, 11, 706-711.
43. J. Jung, T. Sondergaard and S. I. Bozhevolnyi, *Physical Review B*, 2007, 76, 035434.
44. P. Berini, *Opt. Lett.*, 1999, 24, 1011-1013.
45. Y. G. Sun, B. Mayers, T. Herricks and Y. N. Xia, *Nano Letters*, 2003, 3, 955-960.
46. A. Tao, F. Kim, C. Hess, J. Goldberger, R. R. He, Y. G. Sun, Y. N. Xia and P. D. Yang, *Nano Letters*, 2003, 3, 1229-1233.
47. H. Y. Chen, Y. Gao, H. R. Zhang, L. B. Liu, H. C. Yu, H. F. Tian, S. S. Xie and J. Q. Li, *Journal of Physical Chemistry B*, 2004, 108, 12038-12043.
48. Y. Gao, L. Song, P. Jiang, L. F. Liu, X. Q. Yan, Z. P. Zhou, D. F. Liu, J. X. Wang, H. J. Yuan, Z. X. Zhang, X. W. Zhao, X. Y. Dou, W. Y. Zhou, G. Wang, S. S. Xie, H. Y. Chen and J. Q. Li, *Journal of Crystal Growth*, 2005, 276, 606-612.